Depth Dependent Fault Zone Damage in 3D Simulations of Dynamic Rupture on a frictional fault with brittle Damage Breakage Rheology in the bulk Progress Report

Chunhui Zhao[a,b] and Ahmed Elbanna[a, b]

1 Background

Earthquakes and fault zones exhibit complex multi-scale, multi-phase interactions that govern source physics but remain poorly understood. Fault damage zones influence nucleation, rupture propagation, energy partitioning, and arrest, while earthquakes in turn generate co-seismic off-fault damage that modifies fault zone geometry, elasticity, and rheology. The understanding of this co-evolution is hindered by sparse near-fault observations: seismic and geodetic inversions rely on far-field data and linear elastic assumptions that cannot resolve near-fault inelastic response or fine-scale heterogeneity. Furthermore, depth-dependent variations in overburden stress, pore pressure, and seismic properties (Vs, Vp, ρ) likely exert first-order controls on rupture dynamics, ground motion, and low-velocity zone evolution.

Field and high-resolution studies report non-unique damage-zone structures. Part of this disagreement reflects definitional inconsistency: damage zone is defined by seismicity distribution, low-velocity fault zones from tomography, or fracture density from geology, and part reflects genuine hierarchical structure across scales. Reconciling these observations requires 3D physics-based modeling, yet existing 3D fault-zone simulations almost exclusively use elastoplastic rheology, which cannot capture the elastic-modulus reductions documented in lab experiments and field studies. The few 3D damage-rheology models are either quasi-static or use depth-invariant stress profiles, and prior 2D plane strain studies cannot represent stress redistribution and rupture-front distortion that arise from non-uniform damage across depth.

We perform 3D dynamic rupture simulations on a preexisting fault governed by linear slip-weakening friction, with off-fault response described by a continuum damage-breakage (CDB) rheology that tracks both cracking and granulation state variables, captures elastic-modulus evolution, and transitions spontaneously to granular flow at critical damage. The simulations consider effects with depth-dependent properties and strain rate dependent damage accumulation. This framework lets us examine how damage-zone structures evolve during rupture, identify the controlling factors behind their variability, and connect the simulations to field observations of fault damage architecture.

2 Problem Setup

A static solver establishes initial equilibrium and resolves the depth-dependent stress gradient, dynamic solver then uses the resultant field as initial condition for dynamic rupture simulation. As shown in Figure 1[1], boundary traction T is applied consistent with the prescribed stress field, while an eigenstrain field converted from the initial stress guides the system toward the target solution; rigid body motion is eliminated by constraining the four corner points in all directions and fixing the bottom boundary in z. The procedure and the resultant fields are verified against the SCEC TPV26 benchmark. Figure 1[2] shows the resulting depth profiles of seismic properties (Vs, Vp, ρ), effective stress (σ′), and the initial strain invariant ratio ξ(t = 0) for three cases. Case 1 (baseline) uses depth-constant seismic properties and a linearly varying effective stress down to 15 km, yielding linearly depth-varying on-fault shear stress and strength and a depth-uniform ξ(t = 0). Case 2 introduces an overpressurized zone

between 7–15 km, producing depth-constant effective normal and on-fault shear stresses within that interval. Case 3 adopts a 1D velocity structure with reduced seismic properties near the free surface (following SCEC Benchmark TPV32), yielding a depth-varying ξ(t = 0) that, as shown later, exerts a deterministic influence on the off-fault damage pattern. The problem setup is summarized in Table 1.

Case	Pore Pressure Condition	Material Properties	Notes
1	Constant hydrostatic pore pressure	Constant with depth (uniform)	Baseline reference case
2	Hydrostatic-to-lithostatic transition	Constant with depth (uniform)	Effect of pore-pressure transition
3	Constant hydrostatic pore pressure	1D velocity structure (depth-dependent)	Effect of seismic property variation

Table 1: Summary of simulation cases considered in this study.

3 Results

3.1 3D Damage pattern and spatial heterogeneity

Figure 3 presents selected time snapshots of off-fault damage evolution, where the gray surfaces denote 2D fault plane and iso-contours of high breakage state ($B > 0.8$). As indicated in Figure 2(a)[1], the fault plane is oriented such that the tensile side (”T”) where the off-fault damage preferentially develops, is visible for direct observation. The continuum damage-breakage model predicts high breakage states reduce the effective shear modulus μ_{eff}, decrease the shear wave speed ratio c_s/c^o_s value. Regions exhibiting reduced wave speed are thus identified as the fault damage zone, which creates a strong modulus contrast compared with the surrounding medium. Figure 2(a) illustrates the damage evolution pattern for Case 1, which assumes a depth-constant seismic properties and linearly varying effective stress profile. Damage band evolution appears on the tensile-side (”T”) off-fault medium, initiates as short, curved branches (see Figure 2(a)[1]) that progressively coalesce (see Figure 2(a)[2]-[4]), producing a spatially asymmetric damage pattern. These off-fault bands appear repetitive, staggered, and discontinuous along strike. In contrast, Figure 2(b) highlights markedly different structures in Case 2, with constant stress drop due to over-pressurization: damage zones extend throughout the depth, and the associated off-fault branches are long, straight, and vertically continuous. Such depth-invariant damage patterns have been reported in recent field studies, and may be explained by a depth-independent stress drop due to fluid pressurization that smears the depth variation of off-fault damage, and yields damage bands of comparable width across depth. Figure 2(c) demonstrates the influence of depth-dependent seismic properties (V_s, V_p, ρ) on damage generation, leading to strong localization in shallower depth, symmetrically around the fault plane. This flower-like structure align with the field observations, and it is determined by the in-depth local strain field, due to introduction of 1D velocity structure, the seismic properties in Case 3 reduces its value near the free surface, generating a tensile strain condition which is plausible for damage accumulation and localization on both sides of the fault. We conclude that the pre-event strain field and stress field have deterministic effects on the off-fault damage pattern.

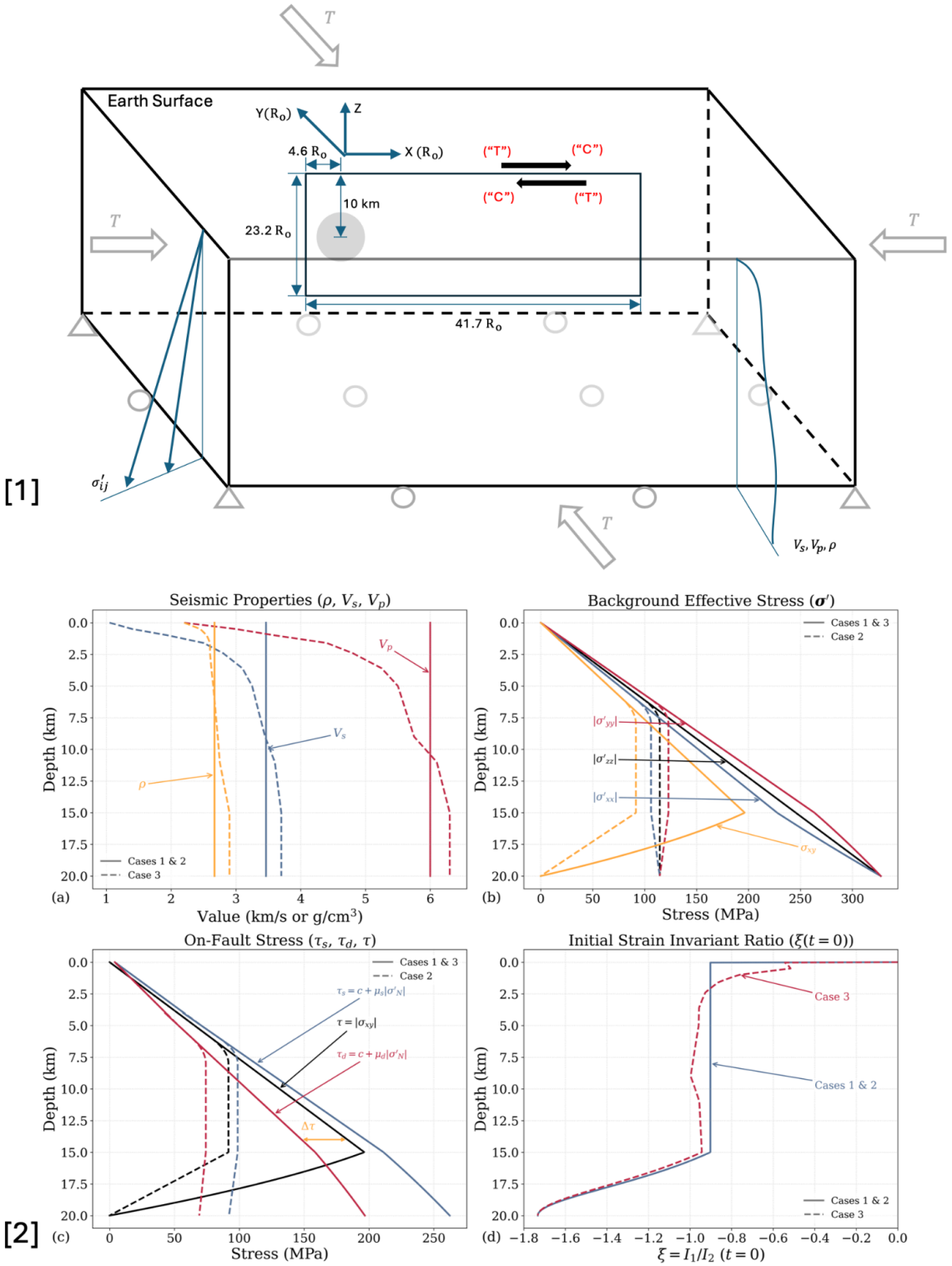

Figure 1: (1) Simulation domain. A 2D fault plane is centered in the domain, with a free surface on top, applied traction T on the sides, and fixed support at the bottom. Rupture nucleates within the gray circular region centered at 10 km depth, with the coordinate origin at the free surface directly above. Black arrows indicate right-lateral strike-slip motion; "T" and "C" mark the off-fault tensile and compressive sides. (2) Depth profiles for the three cases: (a) seismic properties — uniform in Cases 1–2, depth-varying in Case 3; (b) background effective stress — linearly increasing in Cases 1 and 3, with fluid over-pressurization at 7–15 km in Case 2, and reduced shear stress below 15 km reflecting the brittle–ductile transition; (c) on-fault peak and residual shear strengths (τs, τd) from slip-weakening friction and fault-normal stress, with stress drop Δτ = τ − τd driving rupture; (d) strain invariant ratio ξ — depth-uniform in Cases 1–2, elevated near the free surface in Case 3.

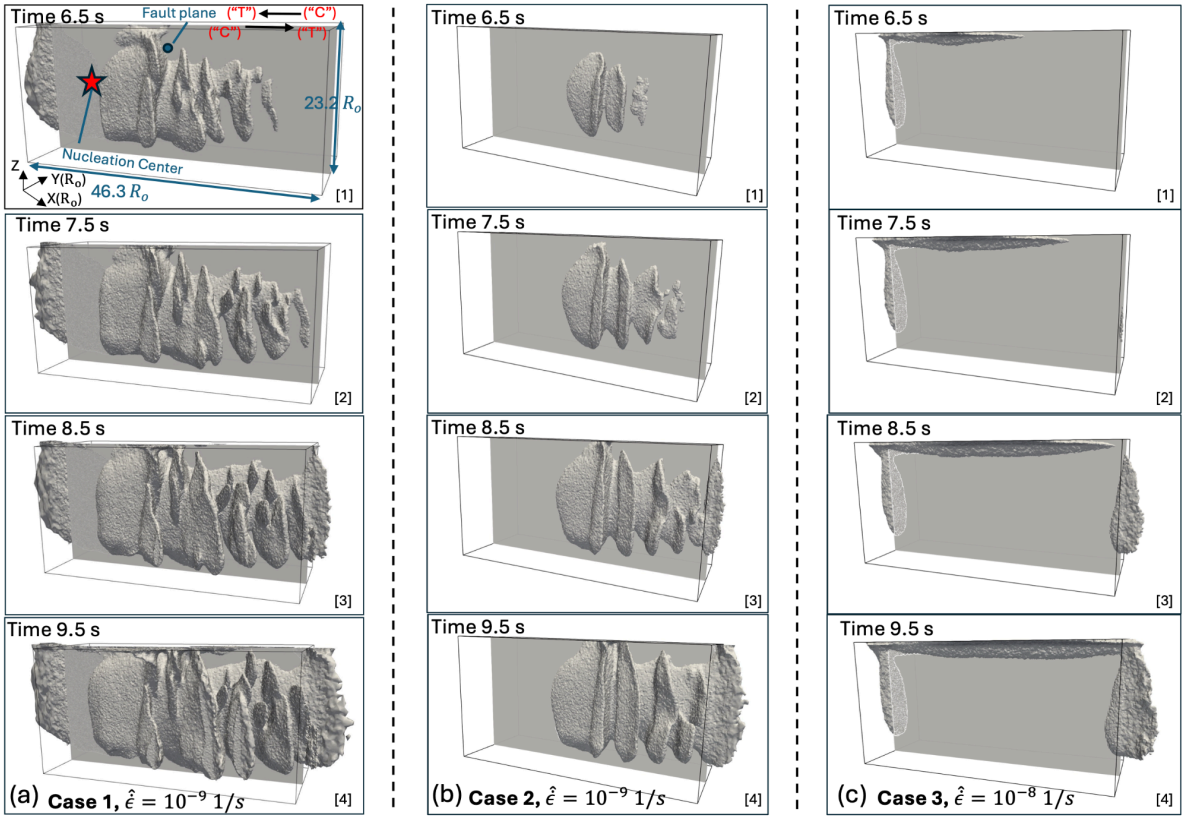

Figure 2: Three-dimensional temporal and spatial evolution of off-fault damage for the three cases. The top panel of (a) at t = 6.5 s shows the model configuration: nucleation center (red star), fault plane (gray surface), slip direction (black arrow), tensile and compressive sides ("T", "C"), and fault length and width scaled by process-zone size Ro. All geometries are iso-surfaces of B > 0.8; the black frame marks the region of interest, not the domain boundaries. (a) Case 1: short, staggered branches form along strike, with localization initiating at depth and propagating upward. (b) Case 2: long, planar branches develop continuously throughout depth, populating the entire tensile side. Both Cases 1 and 2 show discontinuous off-fault fracturing, with isolated branches forming intermittently along the rupture path. (c) Case 3 (depth-dependent seismic properties): damage localizes near the free surface and evolves as a continuous, coherent band before reaching the fault boundary. Unlike Cases 1 and 2, which produce asymmetric damage on the tensile side, Case 3 preserves symmetry across the fault (see Figure 5 for strike-perpendicular slices).

3.2 Effects of stress drop and depth-varying damage structure

Figure 3 illustrates the effect of stress drop by comparing strike slices of Case 1 (hydrostatic pore pressure with linearly increasing stress drop with depth) and Case 2 (over-pressurization with constant stress drop); see also Figure 3(c). Figures 3(a) and 3(b) show the shear wave speed ratio along depth at a strike distance of 20 R_o for the two cases. Along depth, both cases exhibit similar trends: maximum shear wave speed reduction occurs near the free surface, with progressively less reduction at greater depth. In terms of damage zone width, Case 1, which has a higher stress drop, produces a wider damage zone (W = 6 R_o) than Case 2 (W = 3 R_o). However, both cases exhibit depth-independent damage zone width, which is quantitatively distinct from the flower-like structure observed in Case 3. The results suggest that on-fault stress drop, which is directly linked to energy dissipation during rupture, governs the width of damage band growth, rather than the reduced frictional resistance that promotes fault sliding under over-pressurization conditions. The emergence of damage bands, growth and variation along the depth due to the stress redistribution, can only be captured through a

full three dimensional numerical model.

From the shear wave speed ratio plots in Figure 3 (a)-(b), we observe whether the damage zone developed during dynamic rupture possess depth variance or not depends on the definition of ”damage zone”: if we interpret damage zone as grain size distribution (related to breakage variable *B*) or fracture density (related to damage variable *α*), the damage zone doesn't have a clear depth variance. However from a seismic tomography perspective, the low velocity fault zones have the greatest reduction near free surface due to the dominant tensile strain and increased velocity value at greater depth located within the compressive strain state. Our numerical study is able to produce both interpretations within a unified framework.

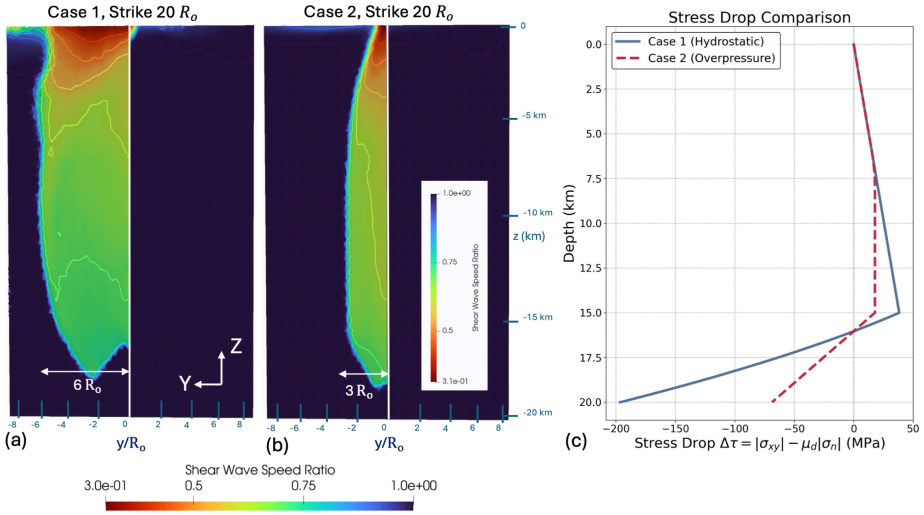

Figure 3: Slice at strike 20 Ro, illustrating the effects of stress drop and depth-independent damage structure, both cases use the same Cd. (a) Case 1 damage zone structure. (b) Case 2 damage zone structure. (c) Comparison of stress drop between Case 1 and Case 2.

5 Discussion and Future Work

We extend our MOOSE-FARMS dynamic rupture simulator to 3D by coupling an off-fault continuum damage-breakage rheology with on-fault linear slip-weakening friction, and use it to investigate how depth-dependent seismic properties and stress profiles govern off-fault damage evolution. The simulations reproduce field-observed asymmetric and symmetric damage patterns, depth-dependent shear-wave-speed reduction, and en echelon fracture geometries or flow-like structures. Damage symmetry is controlled by the competition between the initial stress/strain state and the internal friction angle: ξ(t = 0) < ξo produces classic asymmetric damage on the tensile side, while ξ(t = 0) > ξo near the free surface enables bilateral accumulation and a flower-like structure. Shear-wave-speed reduction in the fully granular state is largest near the surface and diminishes with depth, reflecting the depth-dependent ξ profile inherited through the granular free energy ΨB(ξ). Stress drop, not frictional strength, is the dominant control on damage band morphology and width, with both configurations ultimately developing depth-independent damage patterns.

Future work will extend this framework along four directions: (i) two-way hydro-mechanical coupling via a thermodynamically consistent visco-poro-damage formulation; (ii) earthquake cycle simulations with rate-and-state friction to capture interseismic healing and history-dependent damage evolution; (iii) thermal effects through slip-induced heat generation and temperature-dependent healing parameters; and (iv) better experimental constraints on healing parameters to enable predictive modeling of long-term fault zone recovery.

References

1. Ben-Zion, Y. Collective behavior of earthquakes and faults: Continuum-discrete transitions, progressive evolutionary changes, and different dynamic regimes. *Reviews of Geophysics* 46 (2008).
2. Ben-Zion, Y. & Zaliapin, I. Spatial variations of rock damage production by earthquakes in southern California. *Earth and Planetary Science Letters* 512, 184–193 (2019).
3. Becker, T. W., Hardebeck, J. L. & Anderson, G. Constraints on fault slip rates of the southern California plate boundary from GPS velocity and stress inversions. *Geophysical Journal International* 160, 634–650 (2005).
4. Hardebeck, J. L. & Michael, A. J. Damped regional-scale stress inversions: Methodology and examples for southern California and the Coalinga aftershock sequence. *Journal of Geophysical Research: Solid Earth* 111 (2006).
5. Tse, S. T. & Rice, J. R. Crustal earthquake instability in relation to the depth variation of frictional slip properties. *Journal of Geophysical Research: Solid Earth* 91, 9452–9472 (1986).
6. Zencher, F., Bonafede, M. & Stefansson, R. Near-lithostatic pore pressure at seismogenic depths: a thermoporoelastic model. *Geophysical Journal International* 166, 1318–1334 (2006).
7. Madden, E. H., Ulrich, T. & Gabriel, A.-A. The state of pore fluid pressure and 3- D megathrust earthquake dynamics. *Journal of Geophysical Research: Solid Earth* 127, e2021JB023382 (2022).
8. Rice, J. R. in *International geophysics* 475–503 (Elsevier, 1992).
9. Bem, T. S. *et al.* High-resolution 3-D crustal shear-wave velocity model reveals struc tural and seismicity segmentation of the central-southern Tanlu Fault zone, eastern China. *Tectonophysics* 778, 228372 (2020).
10. Mooney, W. D. & Ginzburg, A. Seismic measurements of the internal properties of fault zones. *Pure and Applied Geophysics* 124, 141–157 (1986).
11. Schliwa, N., Gabriel, A.-A. & Ben-Zion, Y. Shallow fault zone structure affects rupture dy namics and ground motions of the 2019 Ridgecrest sequence to regional distances. *Journal of Geophysical Research: Solid Earth* 130, e2025JB031194 (2025).
12. Ma, S. A physical model for widespread near-surface and fault zone damage induced by earthquakes. *Geochemistry, Geophysics, Geosystems* 9 (2008).
13. Sibson, R. H. Thickness of the seismic slip zone. *Bulletin of the Seismological Society of America* 93, 1169–1178 (2003).
14. Lewis, M., Peng, Z., Ben-Zion, Y. & Vernon, F. Shallow seismic trapping structure in the San Jacinto fault zone near Anza, California. *Geophysical Journal International* 162, 867– 881 (2005).
15. Atterholt, J., Zhan, Z., Yang, Y. & Zhu, W. Imaging the garlock fault zone with a fiber: a limited damage zone and hidden bimaterial contrast. *Journal of Geophysical Research: Solid Earth* 129, e2024JB028900 (2024).
16. Ben-Zion, Y. *et al.* A shallow fault-zone structure illuminated by trapped waves in the Karadere–Duzce branch of the North Anatolian Fault, western Turkey. *Geophysical Journal International* 152, 699–717 (2003).
17. Li, Y.-G. & Vernon, F. L. Characterization of the San Jacinto fault zone near Anza, Cal ifornia, by fault zone trapped waves. *Journal of Geophysical Research: Solid Earth* 106,

30671–30688 (2001).

18. Huang, L. & Liu, C.-y. Three types of flower structures in a divergent-wrench fault zone. *Journal of Geophysical Research: Solid Earth* 122, 10–478 (2017).

19. Savage, H. M. & Rowe, C. D. Localization and delocalization during seismic slip. *Geophysical Research Letters* 51, e2024GL110058 (2024).

20. Rowe, C. & Hatem, A. *How Wide Are Faults?* https://seismosoc.secure-platform.com/a/gallery/rounds/43/details/12592.

21. Li, H., Zhu, L. & Yang, H. High-resolution structures of the Landers fault zone inferred from aftershock waveform data. *Geophysical Journal International* 171, 1295–1307 (2007).

22. McGrath, A. G. & Davison, I. Damage zone geometry around fault tips. *Journal of Structural Geology* 17, 1011–1024 (1995).

23. Kim, Y.-S., Peacock, D. C. P. & Sanderson, D. J. Mesoscale strike-slip faults and damage zones at Marsalforn, Gozo Island, Malta. *Journal of Structural Geology* 25, 793–812 (2003).

24. Rysak, B., Gale, J. F., Laubach, S. E. & Ferrill, D. A. Mechanisms for the generation of complex fracture networks: Observations from slant core, analog models, and outcrop. *Frontiers in Earth Science* 10, 848012 (2022).

25. Rockwell, T. K. & Ben-Zion, Y. High localization of primary slip zones in large earthquakes from paleoseismic trenches: Observations and implications for earthquake physics. *Journal of Geophysical Research: Solid Earth* 112 (2007).

26. Powers, P. M. & Jordan, T. H. Distribution of seismicity across strike-slip faults in California. *Journal of Geophysical Research: Solid Earth* 115 (2010).

27. Yang, H. & Zhu, L. Shallow low-velocity zone of the San Jacinto fault from local earthquake waveform modelling. *Geophysical Journal International* 183, 421–432 (2010).

28. Mitchell, T. & Faulkner, D. The nature and origin of off-fault damage surrounding strike slip fault zones with a wide range of displacements: A field study from the Atacama fault system, northern Chile. *Journal of Structural Geology* 31, 802–816 (2009).

29. Ampuero, J. P. & Mao, X. Upper limit on damage zone thickness controlled by seismogenic depth. *Fault zone dynamic processes: Evolution of fault properties during seismic rupture,* 243–253 (2017).

30. Wollherr, S., Gabriel, A.-A. & Uphoff, C. Off-fault plasticity in three-dimensional dynamic rupture simulations using a modal Discontinuous Galerkin method on unstructured meshes: implementation, verification and application. *Geophysical Journal International* 214, 1556– 1584 (2018).

31. Finzi, Y., Hearn, E. H., Ben-Zion, Y. & Lyakhovsky, V. Structural properties and deformation patterns of evolving strike-slip faults: Numerical simulations incorporating damage rheology. *Pure and Applied Geophysics* 166, 1537–1573 (2009).

32. Niu, Z., Gabriel, A.-A. & Ben-Zion, Y. Delayed dynamic triggering and enhanced high frequency seismic radiation from brittle rock damage in 3D dynamic rupture simulations. *Journal of Geophysical Research: Solid Earth* 130, e2025JB031632 (2025).

33. Ben-Zion, Y. & Sammis, C. G. Characterization of fault zones. *Pure and applied geophysics* 160, 677–715 (2003).

34. Allam, A., Ben-Zion, Y., Kurzon, I. & Vernon, F. Seismic velocity structure in the Hot Springs and Trifurcation areas of the San Jacinto fault zone, California, from double

difference tomography. *Geophysical Journal International* 198, 978–999 (2014).

35. Zigone, D., Ben-Zion, Y., Campillo, M. & Roux, P. Seismic tomography of the Southern California plate boundary region from noise-based Rayleigh and Love waves. *Pure and Applied Geophysics* 172, 1007–1032 (2015).

36. Qiu, H. *et al.* Seismic imaging of the Mw 7.1 Ridgecrest earthquake rupture zone from data recorded by dense linear arrays. *Journal of Geophysical Research: Solid Earth* 126, e2021JB022043 (2021).

37. Gupta, I. N. Seismic velocities in rock subjected to axial loading up to shear fracture. *Journal of Geophysical Research* 78, 6936–6942 (1973).

38. Lockner, D. & Byerlee, J. Development of fracture planes during creep in granite (1980).

39. Stanchits, S., Vinciguerra, S. & Dresen, G. Ultrasonic velocities, acoustic emission charac teristics and crack damage of basalt and granite. *Pure and Applied Geophysics* 163, 975–994 (2006).

40. Aben, F. M., Brantut, N., Mitchell, T. M. & David, E. C. Rupture energetics in crustal rock from laboratory-scale seismic tomography. *Geophysical Research Letters* 46, 7337–7344 (2019).

41. Xu, S., Fukuyama, E., Yamashita, F. & Takizawa, S. Evolution of fault-interface Rayleigh wave speed over simulated earthquake cycles in the lab: Observations, interpretations, and implications. *Earth and Planetary Science Letters* 524, 115720 (2019).

42. Peng, Z. & Ben-Zion, Y. Temporal changes of shallow seismic velocity around the Karadere D¨uzce branch of the north Anatolian fault and strong ground motion. *Pure and Applied Geophysics* 163, 567–600 (2006).

43. Froment, B., Campillo, M., Chen, J. & Liu, Q. Deformation at depth associated with the 12 May 2008 Mw 7.9 Wenchuan earthquake from seismic ambient noise monitoring. *Geophysical Research Letters* 40, 78–82 (2013).

44. Pei, S. *et al.* Seismic velocity reduction and accelerated recovery due to earthquakes on the Longmenshan fault. *Nature Geoscience* 12, 387–392 (2019).

45. Hamiel, Y., Liu, Y., Lyakhovsky, V., Ben-Zion, Y. & Lockner, D. A viscoelastic damage model with applications to stable and unstable fracturing. *Geophysical Journal Interna tional* 159, 1155–1165 (2004).

46. Xu, S., Ben-Zion, Y., Ampuero, J.-P. & Lyakhovsky, V. Dynamic ruptures on a frictional interface with off-fault brittle damage: feedback mechanisms and effects on slip and near fault motion. *Pure and Applied Geophysics* 172, 1243–1267 (2015).

47. Ben-Zion, Y. & Aki, K. Seismic radiation from an SH line source in a laterally heterogeneous planar fault zone. *Bulletin of the Seismological Society of America* 80, 971–994 (1990). 48. Spudich, P. & Olsen, K. Fault zone amplified waves as a possible seismic hazard along the Calaveras fault in central California. *Geophysical Research Letters* 28, 2533–2536 (2001). 49. Weertman, J. Unstable slippage across a fault that separates elastic media of different elastic constants. *Journal of Geophysical Research: Solid Earth* 85, 1455–1461 (1980). 50. Andrews, D. J. & Ben-Zion, Y. Wrinkle-like slip pulse on a fault between different materials. *Journal of Geophysical Research: Solid Earth* 102, 553–571 (1997).

51. Shlomai, H. & Fineberg, J. The structure of slip-pulses and supershear ruptures driving slip in bimaterial friction. *Nature communications* 7, 11787 (2016).

52. Ben-Zion, Y. & Huang, Y. Dynamic rupture on an interface between a compliant fault zone layer and a stiffer surrounding solid. *Journal of Geophysical Research: Solid Earth* 107,

ESE–6 (2002).

53. Huang, Y. & Ampuero, J.-P. Pulse-like ruptures induced by low-velocity fault zones. *Jour nal of Geophysical Research: Solid Earth* 116 (2011).

54. Ampuero, J.-P. & Ben-Zion, Y. Cracks, pulses and macroscopic asymmetry of dynamic rupture on a bimaterial interface with velocity-weakening friction. *Geophysical Journal International* 173, 674–692 (2008).

55. Bhat, H. S., Biegel, R. L., Rosakis, A. J. & Sammis, C. G. The effect of asymmetric damage on dynamic shear rupture propagation II: With mismatch in bulk elasticity. *Tectonophysics* 493, 263–271 (2010).

56. Thakur, P. & Huang, Y. Influence of fault zone maturity on fully dynamic earthquake cycles. *Geophysical Research Letters* 48, e2021GL094679 (2021).

57. Aichele, J., Latour, S., Catheline, S. & Roux, P. Dynamic full-field imaging of rupture radiation: Material contrast governs source mechanism. *Geophysical Research Letters* 50, e2022GL100473 (2023).

58. Abdelmeguid, M. & Elbanna, A. Sequences of seismic and aseismic slip on bimaterial faults show dominant rupture asymmetry and potential for elevated seismic hazard. *Earth and Planetary Science Letters* 593, 117648 (2022).

59. Ferry, R. & Molinari, J.-F. Do Slip-Weakening Laws Shapes Influence Rupture Dynamics? *arXiv preprint arXiv:2407.14337* (2024).

60. Lyakhovsky, V., Hamiel, Y. & Ben-Zion, Y. A non-local visco-elastic damage model and dynamic fracturing. *Journal of the Mechanics and Physics of Solids* 59, 1752–1776 (2011).

61. Lyakhovsky, V. & Ben-Zion, Y. A continuum damage–breakage faulting model and solid granular transitions. *Pure and Applied Geophysics* 171, 3099–3123 (2014).

62. Lyakhovsky, V. & Ben-Zion, Y. Damage–breakage rheology model and solid-granular tran sition near brittle instability. *Journal of the Mechanics and Physics of Solids* 64, 184–197 (2014).

63. Lyakhovsky, V., Ben-Zion, Y., Ilchev, A. & Mendecki, A. Dynamic rupture in a damage breakage rheology model. *Geophysical Journal International* 206, 1126–1143 (2016).

64. Zhao, C., Mia, M. S., Elbanna, A. & Ben-Zion, Y. Dynamic rupture modeling in a complex fault zone with distributed and localized damage. *Mechanics of Materials* 198, 105139 (2024).

65. Day, S. M., Dalguer, L. A., Lapusta, N. & Liu, Y. Comparison of finite difference and boundary integral solutions to three-dimensional spontaneous rupture. *Journal of Geo physical Research: Solid Earth* 110 (2005).

66. Ba˘zant, Z. P. & Lin, F.-B. Nonlocal smeared cracking model for concrete fracture. *Journal of structural engineering* 114, 2493–2510 (1988).

67. Ba˘zant, Z. P. & Jir´asek, M. Nonlocal integral formulations of plasticity and damage: survey of progress. *Journal of engineering mechanics* 128, 1119–1149 (2002).

68. Lyakhovsky, V., Ben-Zion, Y. & Agnon, A. Distributed damage, faulting, and friction. *Journal of Geophysical Research: Solid Earth* 102, 27635–27649 (1997).

69. Lyakhovsky, V., Ben-Zion, Y. & Agnon, A. A viscoelastic damage rheology and rate-and state-dependent friction. *Geophysical Journal International* 161, 179–190 (2005).

70. Zhai, P., Huang, Y., Liang, C. & Ampuero, J.-P. Fully dynamic seismic cycle simulations in co-evolving fault damage zones controlled by damage rheology. *Geophysical Journal*

International 242, ggaf274 (2025).

71. Harris, R. A. *et al.* A suite of exercises for verifying dynamic earthquake rupture codes. *Seismological Research Letters* 89, 1146–1162 (2018).

72. Palmer, A. C. & Rice, J. R. The growth of slip surfaces in the progressive failure of over consolidated clay. *Proceedings of the Royal Society of London. A. Mathematical and Phys ical Sciences* 332, 527–548 (1973).

73. Harris, R. A. *et al.* The SCEC/USGS dynamic earthquake rupture code verification exer cise. *Seismological Research Letters* 80, 119–126 (2009).

74. Lindsay, A. D. *et al.* 2.0-MOOSE: Enabling massively parallel multiphysics simulation. *SoftwareX* 20, 101202 (2022).

75. Abdelmeguid, M. *et al.* Dynamics of episodic supershear in the 2023 M7. 8 Kahraman mara¸s/Pazarcik earthquake, revealed by near-field records and computational modeling. *Communications Earth & Environment* 4, 456 (2023).

76. Nguyen, V. P. An open source program to generate zero-thickness cohesive interface ele ments. *Advances in Engineering Software* 74, 27–39 (2014).

77. Lysmer, J. & Kuhlemeyer, R. L. Finite dynamic model for infinite media. *Journal of the engineering mechanics division* 95, 859–877 (1969).

78. Veeraraghavan, S. *et al.* MASTODON: an open-source software for seismic analysis and risk assessment of critical infrastructure. *Nuclear Technology* 207, 1073–1095 (2021).

79. Santarossa, A., Varela-Rosales, N. R., Steinmann, P. & Moreno-Mateos, M. A. Configu rational forces explain echelon cracks in soft materials. *arXiv preprint arXiv:2507.12247* (2025).

80. Kim, Y.-S., Peacock, D. C. & Sanderson, D. J. Fault damage zones. *Journal of structural geology* 26, 503–517 (2004).

81. Segall, P. & Pollard, D. Mechanics of discontinuous faults. *Journal of Geophysical Research: Solid Earth* 85, 4337–4350 (1980).

82. Yasuhara, H., Marone, C. & Elsworth, D. Fault zone restrengthening and frictional healing: The role of pressure solution. *Journal of Geophysical Research: Solid Earth* 110 (2005).

83. Boettcher, M. & Marone, C. Effects of normal stress variation on the strength and stability of creeping faults. *Journal of Geophysical Research: Solid Earth* 109 (2004).

84. Bhat, H. S., Rosakis, A. J. & Sammis, C. G. A micromechanics based constitutive model for brittle failure at high strain rates (2012).

85. Liu, H., Kou, S., Lindqvist, P.-A. & Tang, C. Numerical studies on the failure process and associated microseismicity in rock under triaxial compression. *Tectonophysics* 384, 149–174 (2004).